Politecnico di Torino

MASTER'S DEGREE IN MECHATRONICS ENGINEERING

Autonomous Electric Boat Collision Avoidance Based on Artificial Potential Field

Supervisor:

Ing. Mauro BONFANTI

Tutor:

Prof. Stefano MAURO

Ing. Matteo MELCHIORRE

Candidate:

Mario CISTERNINO

A.Y. 2023 / 2024

Table of Contents

List of Tables

List of Figures

Chapter 1

Introduction

1.1 Description of the subject

This thesis was done as part of a project at Politecnico Di Torino aiming in suitably control an autonomous electric boat for transportation on urban canals. Traditionally, the pilot is responsible for planning the path and steering the boat avoiding obstacles while respecting regulations for collision prevention and speed limits. However, human operation is strongly dependent on experience, unpredictable condition, and fate. For this reason, the use of an autonomous electric boat can ensure not only a more predictable and controlled guidance behaviour, but also represents a successful strategy to improve safeguard in maritime application. Moreover, a wide adoption of autonomous boats could increase the efficiency and reduce the chaotic traffic in canals caused by commercial operations.

1.2 Objectives

The objective of this thesis is to develop a control algorithm able to guide an autonomous electric boat in a safe an efficient manner from a start location to a defined goal point being able to autonomously avoiding obstacles and other boats accordingly to the Convention on the International Regulations for Preventing Collisions at Sea, 1972 (COLREGs). The local motion planning is performed using information collected by on-board sensors, for this reason obstacles position and velocity and environment information are assumed to be known. It has been used an existing boat design for simulation, but the evidence demonstrates in this work can be applied to other models with the necessary adjustments.

1.3 Methodology

In the following chapter it is illustrated how the task to ensure safe autonomous guidance has been developed over the recent years to have a general understanding of the progression of the subject. Then, in the third chapter is presented a theoretical overview

of the chosen methodology within the ones presented. It focuses on a particular application able to directly influence the behaviour of the controlled boat to fulfil some of the COLREGs compliance requirements. Further, the next chapter describes the dynamic model used for simulation and the subsequent control problem formulation derived from. In the end, the last chapter shows all the results of the application of the methodology formulated with a particular comparison with a different strategy to highlight strengths and weaknesses. In conclusion, some suggestion to continue developing this work have been emphasized.

Chapter 2

State of the Art

In recent years, unmanned vehicles in dynamic environments are a growing and challenging area of research. They consist in autonomous vehicles able to perform path planning and collision avoidance without human intervention by collecting information about the surrounding environment and taking decisions accordingly.

2.1 Path Planning

Path planning algorithms aim to find a suitable and collision free path from an initial position to a desired goal state. According to Vagale et al. [1] it is possible to distinguish between global path planning and local path planning. While the first one evaluates the preferred path exploiting a priori information such as the position of the static obstacle or information on the environment, the second one utilizes data obtained online by means of sensors and it can adapt the preferable path in real time.

In this section there will be discussed some path planning and collision avoidance methodologies. The Dijkstra's algorithm is a shortest path search algorithm used to find the shortest path between two nodes in a weighted graph, and it is always able to find the minimal cost path, but it lacks in dynamic optimization, and it suffers of high computational cost in large configuration space. This algorithm was modified by Hart et al. in 1972 to create A* which utilizes a heuristic function to evaluate the total cost to reach the destination through each reachable node with the minimal cost. A* (HA*), unlike conventional variants that only allow visiting centres, corners, or edges of grid cells, associates with each cell a continuous state of vehicles [2] (Dolgov et al., 2008, in Miao, 2022). This method suffers from similar weaknesses as the previous one plus the uniqueness of the solution, so if more than one optimal path comes out it will arbitrary chose one of them without providing insights into alternative routes. Commonly, when dealing with autonomous guidance it is necessary to follow an approach able to handle with dynamic environment. In these cases, an algorithm such as D* is more suitable since it follows an incremental search type of process able to continuously refine the path based

on new information making it a valid tool for tasks such as robotic navigation. Despite the wild use of this methods the complexity of search algorithms increases with the dimension of the configuration space which is not ideal. In contrast, sampling-based algorithms generate path by randomly sampling points in a surrounding space to determine the validity or accessibility of those positions. In the meantime, this process may include checking for collision with obstacles, boundary limits or environmental obstruction. In such regard one of the most commonly implemented algorithm is the Rapidly-Exploring Random Trees (RTT), proposed by LaValle in 1998 [3] which biases the exploration towards the goal region, the algorithm may occasionally select the goal configuration as the random sample with a certain probability. This algorithm starts from a single node that represents the starting configuration and subsequently it randomly selects a configuration in the space to expand the existing tree moving the object towards the selected configuration for each iteration. Moreover, for each step size the algorithm checks eventual collision with obstacle, the path from the current node to the new one is added to the existing tree only if it assessed to be collision-free so that an edge connecting it to the nearest node in the tree is created. Next, to bias the exploration towards the goal region, the algorithm may occasionally select the goal configuration as the random sample with a certain probability. Finally, when it is added to the tree a node sufficiently close to the goal region, or when a specified maximum number of iterations is reached the algorithm stops and proceeds to the path extraction backtracking from the goal node to the start node along the edges of the tree. Karaman and Frazzoli [4] proposed in 2011 an enhanced version of RRT called RRT* that ensures asymptotic convergence to the optimal path. It develops a node reorientation strategy to adapt the tree to new information suitable for dynamic environments with the opportunity to deal with additional constraints. A subsequent implementation of this strategy is the Dubins- RTT* with a Dubins curve steering function that is capable to generate low-cost paths suitable for curvature constrained vehicles [5]. Specifically, Dubins curves provide the shortest paths between two configurations for vehicle with differential constraints, moreover it is noticed that these trajectories result generally smoother. Long Chen [6] in 2020 implemented a Fuzzy-Kinodynamic RRT, method which generates dynamic path based on the traditional rapidly exploring random tree (RRT) algorithm. Fuzzy logic is a soft computing method and can make use of knowledge expressed in the form of linguistic rules combined with the ability

to handle unknown conditions and react dynamically. By combing Kinodynamic RRT and Fuzzy logic, it is possible to make use of the obstacle avoidance ability in unknown environment and utilize the Kinodynamic RRT to generate the initial path which can be optimized later by the combination method.

2.2 Trajectory Tracking

In this section it will be discussed a background of the research on trajectory tracking and collision avoidance system (COLAV), outlining the latest developments within the USV technology and the very current trends in embracing autonomous vehicles. Various types of controllers exist for Unmanned Surface Vehicles (USVs). Some of these controllers are programmed to obey the International Regulations for Preventing Collisions at Sea (COLREGs). These regulations ensures that all mariners follow standard rules when using water ways and help prevent collision between different vessels in the sea.

The simplest control strategies are not able to consider dynamics and limitations of the boat, this is the case of PID. This linear controller is simple to tune, and it can be applied for trajectory tracking by using two PID controllers tuned separately for longitudinal and lateral tracking [7]. This approach is limited for USV implementations since its performance with nonlinear dynamics is poor and it does not always produce feasible solutions. Khatib [8] introduced in 1985 the artificial potential field (APF) algorithm, The idea is based on a control law designed from a scalar function, the so-called Artificial Potential Field (APF), that shows high-potential regions nearby the obstacles and low-level potential at the goal, this algorithm and its development will be further discussed in the following chapter. Subsequently, the velocity obstacle (VO) approach has been adopted by several researchers for moving hazard avoidance. Since it was first proposed in 1998 for robot motion planning by Fiorini and Shiller, several extensions to VO have been made, including a cooperative form of collision avoidance [9] or probabilistic velocity obstacles [10]. VO approaches generate a cone-shaped obstacle in the velocity space and ensure that there will be no future collisions as long as the robot's velocity vector is outside the VO. Kuwata's et al. [11] elaborate presents an autonomous motion planning algorithm to navigate safely in dynamic and cluttered environments. The algorithm not only guarantees obstacle avoidance for static and moving obstacles, but also applies the international Regulations for Preventing Collisions at Sea adding specific

sets of constraints in the velocity space when the USV is in certain COLREGS situations. On the other hand, the most widely used method for autonomous guidance control is the Model Predictive Control strategy (MPC). MPC is a general and powerful method that can compute optimal trajectories where environmental forces are easily included, and risk, hazard, and operational constraints along with mission objectives can be formalized in the cost function. Usually, it begins with the development of a dynamic model of the system being controlled, it typically incorporates physical laws, system dynamics, and constraints. MPC operates over a finite prediction horizon, which defines the time horizon over which future system behaviour is predicted. The length of the prediction horizon determines how far into the future the controller looks to make decisions. In addition, at each control time step, MPC solves an optimization problem over the prediction horizon to determine the optimal control inputs. The objective of the optimization problem is to minimize a cost function that penalizes deviations from desired setpoints, control inputs, and constraints.

Hagen et al. [12] proposed a COLAV strategy based on MPC that depends on transitional costs in the MPC objective for collision avoidance manoeuvres that are being executed by the marine vessel. These transitional cost aim to increase the incentive to continue an already started COLREGS manoeuvre and alleviate the oscillating behaviour that occur when different COLREGS situations rapidly shift. Further, it is possible to combine to a MPC controller a collision risk assessment [13]. Nevertheless, in case of an USV application it is recommended to rely on a nonlinear model both for accuracy in considering nonlinear behaviour such as hydrodynamics, wave or varying environmental conditions, and for flexibility in representing a wider range of operating conditions.

This work takes the lead from a project based on a Nonlinear MPC controller implemented with an RTT* Dubins curves. It is enriched with a path post processing pouring method effective in shortening the path and in making the path smoother and more continuous, removing abrupt changes in direction. This process leads to a reference trajectory derived from the global path planning. Next, it is introduced a smooth trapezoidal reference velocity profile. In this profile the acceleration and deceleration occur only at the start and end of the trajectory, while the rest of the trajectory is kept at a constant cruise velocity. This is useful because the Dubins curves used during path planning assume a vehicle moving at constant speed, which would be the cruise velocity.

This procedure is known as Trajectory planning and basically consists of binding a time law to a path. Regarding the local motion controller, the controller resulted able to consider constraints representing walls, static and dynamic obstacles such that the boat does not collide during its trajectory and reaches the goal state with near zero errors on the final pose. Nevertheless, aspect such as COLREGS compliant and direct possibility of choosing the preferential avoidance directions are not attainable with such implementation. In the next chapter it will be illustrated a methodology that aims to meet those requirements.
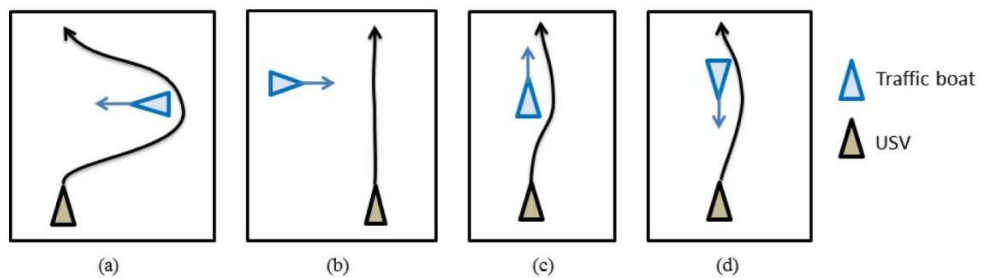

Figure 2.1: Maneuvers required for various COLREGS situations (a) Crossing from right. (b) Crossing from left. (c) Overtaking. (d) Head-on. Extracted from [11].

Chapter 3

Artificial Potential Field with local attractors

This section outlines the formulation of the artificial potential field problem, focusing on scenarios with local attractors. The objectives include achieving a desired position from a given starting configuration, navigating around obstacles while favouring the direction through local attractors and preventing entrapment in local minima associated with these local attractors. The methodology is presented within a two-dimensional space $\mathbb{R}2$. The potential field is constructed using a combination of quadratic and exponential functions, drawing from works from works by Beard & McClain [14] and Khatib [8]. Consequently, considerations regarding the determination of attractor strength are provided.

In [15] Latombe describes the potential function as the sum of the attractive potential and repulsive potential energies acting on the robot. The robot, which is treated as a point in the configuration space, is pulled by the attractive potential toward a defined target and pushed away from obstacles by the repulsive potential. The potential field forces are shown in Figure 3.1.
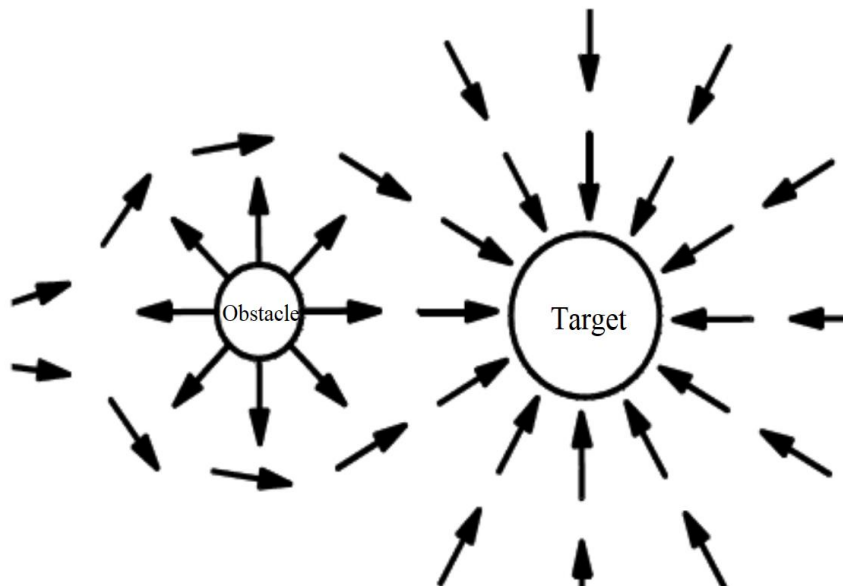

Figure 3.1: Potential field forces orientation. Extracted from [21].

The problem formulation refers to the work presented in [16] where the desired position can be seen as an attractive potential field U_d which is modelled with the quadratic function:

$$Ud(x) = \frac{1}{2}\sigma||x - x_d||^2 \tag{3.1}$$

where σ is a positive parameter which regulates the intensity of the quadratic function and $x = [x\ y]^T$ represent the generic point in the cartesian space.

3.1 Obstacle formulation

In general, obstacles may have any geometry but, in this work, it will be considered only object with the form of disc in two dimensions centred in x_o with radius R_o. Regardless of the obstacle potential formulation it will be formulated with the exponential function according to [14] defined as:

$$Uo(x) = \beta_o e^{-\frac{\gamma_o}{2}||x-x_o||^2} \tag{3.2}$$

In this expression, βo and γo represent positive parameters governing the characteristics of the Gaussian distribution surrounding the obstacle. Specifically, βo signifies the peak value, while γo dictates the rate of exponential decay.
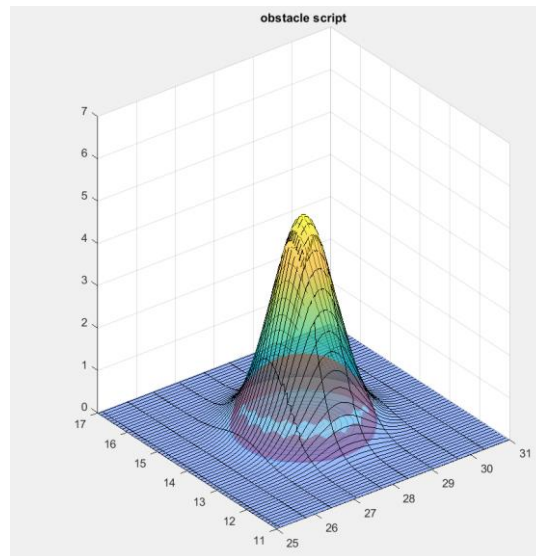

Figure 3.2: Shape of the exponential function defining obstacle potential field.

If only the goal and the obstacle are considered, the resulting total potential field U_{do} can be written as:

$$U_{do}(x) = U_d(x) + U_o(x) = \frac{1}{2}\sigma||x - x_d||^2 + \beta_o e^{-\frac{\gamma_o}{2}||x-x_o||^2} \tag{3.3}$$

The active region U_o^* is defined as the area included in the outer circle with radius R_o^* as described in Figure 3.3a so that the gradient of U_o goes to zero outside U_o^*. Gradient of U_o can be defined as:

$$\Delta U_o(x, \beta_o, \gamma_o) = \frac{\partial}{\partial x}U_o(x, \beta_o, \gamma_o) = -\beta_o\gamma_o(x - x_o)e^{\frac{\gamma_o}{2}||X-X_o||^2} \tag{3.4}$$

More precisely, considering $r_o = ||x - x_o||$ and assuming that the gradient magnitude of the function above is less or equal to a small value defined as s_ε, after same calculation explained in more detail in [16], it is possible to assume that:

$$R_o^* = \left[-\frac{1}{\gamma_o}W_{-1}\left(-\frac{s_\varepsilon^2}{\beta_o^2\gamma_o}\right)\right]^{1/2} \tag{3.5}$$

Where W_{-1} is the Lambert function.
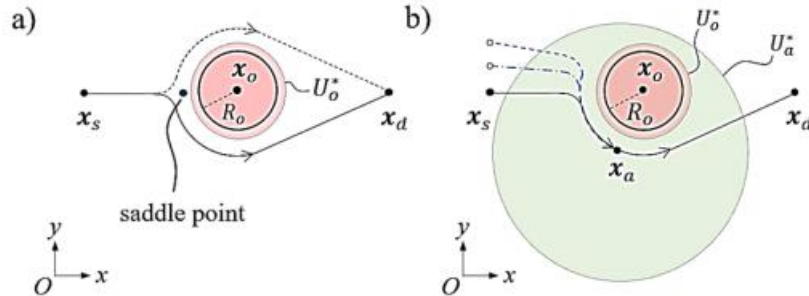
Figure 3. 3: Two-dimensional analysis of the possible USV path. From [16].

3.2 Local attractor formulation

According to [16], the idea is to introduce an attractive source near to the obstacle able to influence the total potential field to create preferable path to be followed in the collision avoidance mechanism. To do so, let be considering now on the local attractor position as x_a and the global attractor position, previously considered as goal point, as x_d.

The local attractor potential field U_a is modelled with the negative exponential function [4]:

$$U_a(x) = -\alpha_a e^{-\frac{\gamma_a}{2}||x-x_a||^2} \tag{3.6}$$

where α_a and γ_a are the positive parameters that regulate the intensity and the decay of the attractive effect. As it is shown in Figure 3.3b the outer circle centred in x_a with radius R_a^* define the active U_a^* so that the gradient of U_a goes to zero outside U_a^*. Similarly with the formulation of the obstacle is it possible to define a small value $s\varepsilon$ equal to the magnitude of the gradient of U_a to impose this condition that leads to:

$$R_a^* = \left[-\frac{1}{\gamma_a}W_{-1}\left(-\frac{s_\varepsilon^2}{\alpha_a^2\gamma_a}\right)\right]^{\frac{1}{2}} \tag{3.7}$$

moreover, the attractor can be located on the chosen side of the obstacle and its active region U_a can be extended all around the obstacle and its active region. Parameter such as α_a and γ_a, if correctly selected, can prevent the total potential field, which in case of single obstacle and in presence of two attractive source can be defined as:

$$U_t(x) = U_d(x) + U_o(x) + U_a(x) =$$
$$= \frac{1}{2}\sigma||x-x_d||^2 + \beta_o e^{-\frac{\gamma_o}{2}||x-x_o||^2} - \alpha_a e^{-\frac{\gamma_a}{2}||x-x_a||^2} \tag{3.8}$$

to suffer of local minima. More precisely, high values of α_a can generate attractive source too intense creating a local minimum, near this point the resultant force experienced by the USV oscillates around zero. In addition, x_a should be sufficiently far from the active region of the obstacle U_o^* otherwise their potential field would interfere with each other making the control action less effective or in the worst-case scenario create an area where the total gradient may result near to zero. This leads to the following condition to be hold:

$$||x_a - x_o|| > R_o^* + \varepsilon \tag{3.9}$$

According do [16], to define ε it is convenient to consider the function U_{da} defined as the sum of the two potential fields of the attractors:

$$U_{da}(x) = U_d(x) + U_a(x) = \frac{1}{2}\sigma||x-x_d||^2 - \alpha_a e^{-\frac{\gamma_a}{2}||x-x_a||^2} \tag{3.10}$$

Since condition (3.9), to understand the influence and the limit value of α_a it is necessary to analyse the points where the gradient of the function U_{da} is zero, the condition becomes:

$$\frac{\partial}{\partial x} U_{da}(x) = \sigma(x - x_d) + \alpha_a \gamma_a(x - x_a)e^{\frac{-\gamma_a}{2}||x - x_a||^2} = 0 \qquad (3.11)$$

Moreover, the problem can be further simplified by defining the auxiliary reference frame O'-x'-y' with the origin in O'$\equiv x_d$ and whose x' axis is aligned with x_a and by considering $x'_d = [0\ 0]^T$ and $x'_a = [x'_a\ 0]^T$. In addition, the problem of interest can be studied in one dimension regarding x' axis only since the partial derivative of U_{da} with respect to y' is equal to zero only for y' = 0 since α_a, σ and γ_a are positive values. Thus, the equation becomes:

$$\frac{\partial}{\partial x'} U_{da}(x', 0) = \sigma x' + \alpha_a \gamma_a(x' - x'_a)e^{\frac{-\gamma_a}{2}(x' - x'_a)^2} = 0 \qquad (3.12)$$

Selecting σ, x_a' and γ_a equation (3.12) is parametric in α_a and this can be visualized in Figure 3.4 by considering:

$$A = \sigma x'\ ;\ B = \alpha_a \gamma_a(x' - x'_a)e^{\frac{-\gamma_a}{2}(x' - x'_a)^2} \qquad (3.13)$$

the graphical solution is shown in Figure 3.4. The objective is to find a small value of α_a for which the curves -A and B have only one intersection and for which $U_{da}(x', 0)$ shows a saddle point in $x' = \tilde{x}'$, that value represents the upper bound $\alpha_{a,lim}$.
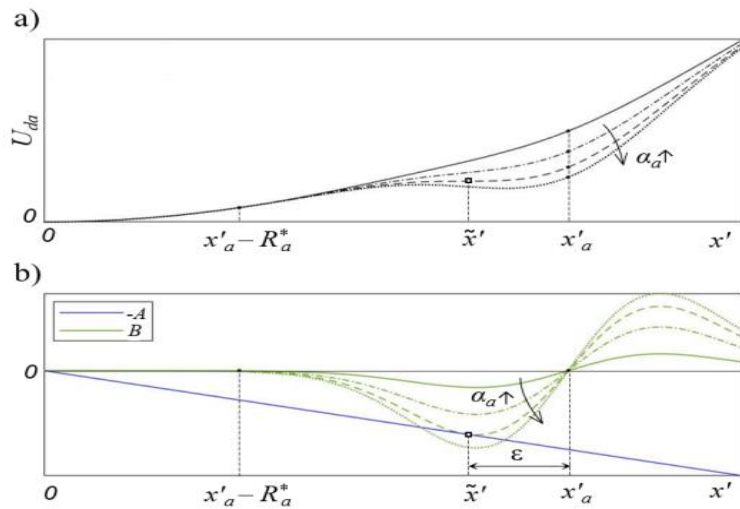

Figure 3. 4: Parametric solution of equation (3.12). Extracted from [16].

As it is shown in Figure 3.4 the shifting can be quantified as the distance:

$$\left|\left|x_a' - \tilde{x}'\right|\right| = x_a' - \tilde{x}' = \varepsilon \qquad (3.14)$$

It is possible to distinguish between two different scenarios. In the first one the intersection between the line segment $x_a x_d$ and U_o^* is empty; in this case the stationary point would fall outside U_o^*. The second case arises when the line segment $x_a x_d$ intersects U_o^*. In the latter, it is important the role of the shifting parameter since it is possible to have the saddle point of U_{da} overlapping with the obstacle if condition (3.9) is not satisfied. To summarize, the value of ε in condition (3.9) is resumed as follow:

$$\begin{array}{ll} \tilde{\varepsilon} = 0 & if \ \overline{x_a x_d} \cap U_o^* = 0 \\ \tilde{\varepsilon} = \varepsilon & if \ \overline{x_a x_d} \cap U_o^* \neq 0 \end{array}$$

Figure 3. 5: Condition on ε [16].

In addition, to regulate the size of U_a^* so that the two potential field do not enter in contrast causing perturbations in the global minimum of the potential, defined in the beginning as the target attractor, the following condition must be held:

$$\left|\left|x_a - x_d\right|\right| \geq R_a^* \qquad (3.15)$$

In Figure 3.6 is described a generic scenario in which conditions (3.9) and (3.15) are satisfied:
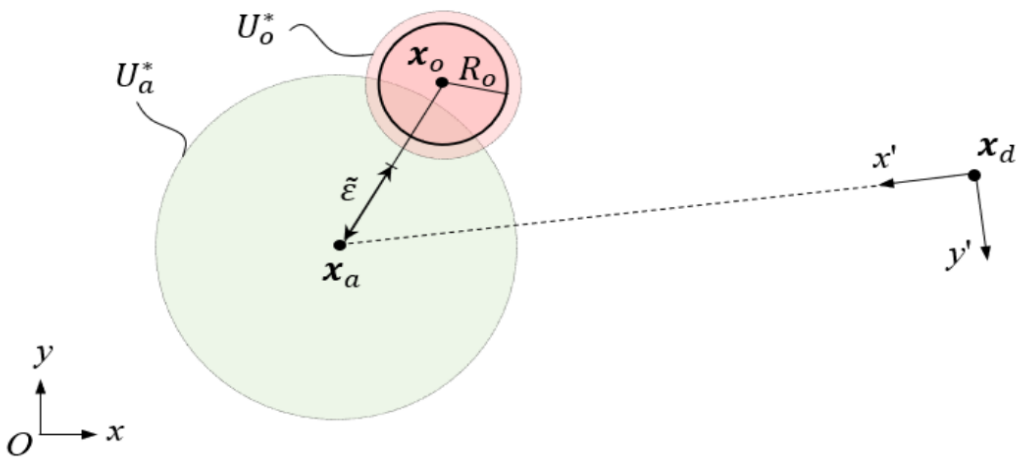

Figure 3. 6: Simple case of obstacle and local attractor positioning. Extracted from [16].

More details about these will be discussed in chapter 5.

Chapter 4

Modelling

This chapter seeks to present the chosen model for simulating and controlling autonomous electric boats. Perez's work [17] has extensively covered ship dynamics theory and various models for both underwater and surface vehicles. Specifically, we will introduce the relevant reference frames and the nonlinear differential equation governing the boat's dynamics.

4.1 Reference Frames

A ship can move in six degrees of freedom (6DOF), three of them describe translations along tree axis and the three coordinates define the orientation. These coordinates can be represented in different standard reference frames:

- North-east-down frame (NED) is a reference frame anchored to the Earth's surface using latitude and longitude coordinates. The n-frame (o_n, x_n, y_n, z_n) has its axis are oriented towards True North, East and Down to the centre of Eart, respectively. This frame is assumed to be inertial, which is reasonable given the low velocities of marine vehicles.
- Body-fixed frame (o_b, x_b, y_b, z_b) is affixed to the hull of the boat. Its positive x_b axis aligns with the bow, the positive y_b axis with starboard, and the positive z_b axis points downward aligned with the normal axis.

Since trajectory tracking disregards vertical translation along the Z-axis, this axis becomes unnecessary for further analysis. Consequently, only a 2D representation of reference frames will suffice. Moreover, rotations around the x_b and y_b axes are deemed insignificant and thus omitted. Both NED and Body-fixed frame are shown in Figure 3.1. The pose of the boat, η, is represented in NED coordinates and indicate the configuration of its position and attitude, while the velocity vector v and the force and momentum vector τ are considered in the Body-fixed frame.

$$\eta = \begin{bmatrix} N \\ E \\ \varphi \end{bmatrix} \qquad v = \begin{bmatrix} u \\ v \\ r \end{bmatrix} \qquad \tau = \begin{bmatrix} X \\ Y \\ N \end{bmatrix} \tag{4.1}$$
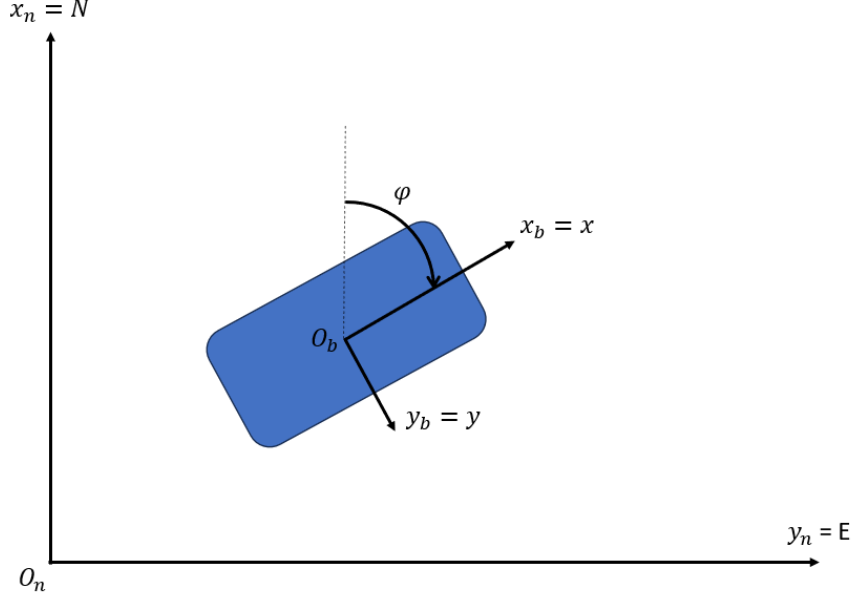

Figure 4. 1: Global and Body-fixed frames.

The angle φ in vector η represent the yaw angle between NED and Body-fixed frame.

4.2 USV Model

In this section, it will be discussed the kinematic model and dynamic model of the USV under three degrees of freedom. The three-degree-of-freedom kinematics model of the unmanned vehicle in plane motion can be expressed as:

$$\dot{\eta} = \begin{bmatrix} cos\varphi & -sin\varphi & 0 \\ sin\varphi & cos\varphi & 0 \\ 0 & 0 & 1 \end{bmatrix} v \tag{4.2}$$

The autonomous electric boat considered in the simulations is based on the ROBOAT II [18] whose dynamic follows the nonlinear differential equation:

$$M\dot{v} + C(v)\,v + D(v)v = \tau \tag{4.3}$$

Where M is the mass matrix, C is the Coriolis and centripetal matrix that considers hydrodynamic coefficients, D is the matrix of hydrodynamic damping. This model assumes that current velocity and both wind and wave force are negligible since their low

value in canals. According to [18], the ROBOAT II has a length of two meters and a width of one meter and the matrices described above are the following:

$$M = diag\{m_{11}, m_{22}, m_{33}\} \tag{4.4}$$

$$C(v) = \begin{bmatrix} 0 & 0 & -m_{22}v \\ 0 & 0 & m_{11}v \\ m_{22}v & -m_{11}v & 0 \end{bmatrix} \tag{4.5}$$

$$D(v) = diag\{X_u, Y_u, N_r\} \tag{4.6}$$

Where, $m_{11} = 172$ kg, $m_{22} = 188$ kg, $m_{33} = 24$ kg·m2, $X_u = 38$ kg/s, $Y_u = 168$ kg/s and $N_r = 16$ kg·m2/s. The boat described used for simulation have two thrusters located as shown in Figure 4.2 at the stern. One is designed to generate longitudinal acceleration along the surge direction, while the other one is designed to steering the boat. Since its distance from the centre is exactly one meter and it is considered the positive direction of rotation the clockwise rotation in the hand righted reference frame, the force and moment vector τ can be rewritten as follows:

$$\tau = \begin{bmatrix} X \\ Y \\ N \end{bmatrix} = \begin{bmatrix} X \\ Y \\ -Y \end{bmatrix} \tag{4.7}$$
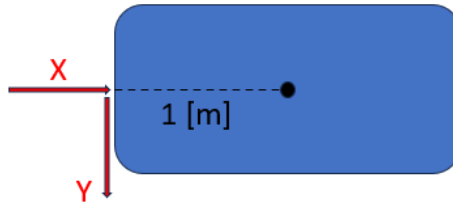

Figure 4. 2: Actuators position on the USV.

Further, it is considered the nonlinear state space form composed by equation (4.2) and (4.3) with state variable $x \in \mathbb{R}^6$, where $x = [\eta^T, v^T]^T = [N, E, \varphi, v_x, v_y, r]^T$, and with u as the input vector. Thus, the nonlinear ODE derived from the state space form and the description of the kinematic and dynamic model are:

$$\frac{d}{dt}\begin{bmatrix} N \\ E \\ \varphi \\ u \\ v \\ r \end{bmatrix} = \begin{bmatrix} u\cos\varphi - v\sin\varphi \\ v\cos\varphi + u\sin\varphi \\ r \\ \dfrac{X}{172} - \dfrac{19u}{86} + \dfrac{47vr}{43} \\ \dfrac{Y}{188} - \dfrac{42v}{47} - \dfrac{43ur}{47} \\ \dfrac{-Y}{24} - \dfrac{2r}{3} - \dfrac{2uv}{3} \end{bmatrix} \qquad (4.8)$$

4.3 Control Problem Formulation

In this section it will be discussed the control problem formulation based on the artificial potential field theory examined above, the same approach is valid for both static and dynamic obstacles. In 1995 Guldner and Utkin [19] elaborated a gradient tracking method able to generate an exact tracking of the gradient lines that can be applied to smooth artificial vector field. The variable under control in this case of study will be the force vector F_d computed as the negative direction of the gradient of the total potential artificial field U_d:

$$F_d = -\nabla U_t \qquad (4.9)$$

The force command is chosen proportional to the error angle created between the actual yaw angle φ of the boat and the direction of the force vector computed at the following control step. Let's consider the angle θ as the angle between the direction of the force vector at instant $t = t_{i+1}$ and the positive direction of the E axis of the NED reference system as it is shown in Figure 4.3. Then, the control angle γ_d is computed as follows:

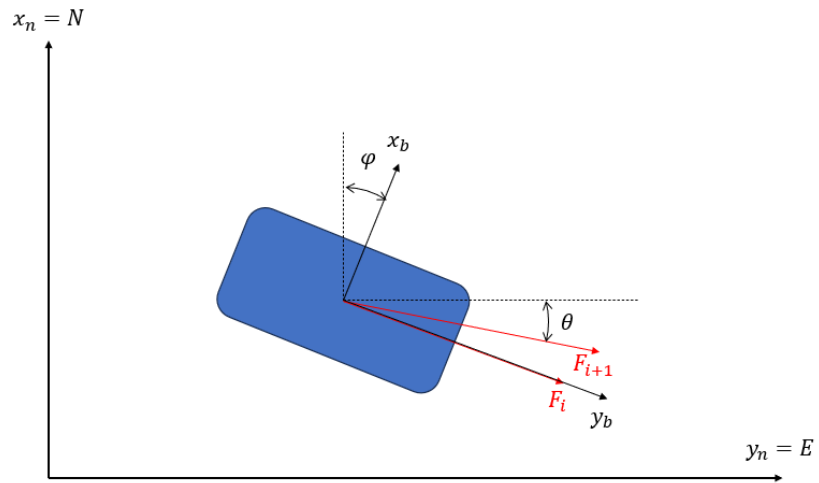$$\gamma_d = \theta - \varphi \qquad (4.10)$$

Figure 4. 3: Error angle

Once the force F_d is computed as in (4.9), the input forces expressed in (4.7) to apply to the boat are distinguished in the longitudinal input force X computed as the modulus of F_d, related to the forward motion, and the steering force Y considered proportional to the control angle γ_d through a constant K:

$$X = norm(F_d) \qquad (4.11)$$

$$Y = -K\gamma_d \qquad (4.12)$$

Chapter 5

Results and Discussion

This chapter is divided in two sections about the performance testing of the collision avoidance system in two real case scenarios. The algorithm is tested on a rectilinear section of the canal considering the presence of two distinct static obstacles in the first case and the frontal approach of a dynamic hazard in the second case. It will be evaluated not only the collision avoidance performance but also the COLREGs rule compliance related to those situations. Results will be compared to a NMPC RTT* integrated with Dubins curves algorithm [20] discussed in the previous chapter. Further, in each section the first part consists of the APF functions formulation whose parameters are tuned to accomplish all the conditions discussed in chapter 3. Then, the control problem parameters are tuned by trial and error until the best performance conditions are reached.

5.1 Case 1: two static obstacles

In the next table are illustrated the first important parameters considered for the simulation, especially the positions expressed in the global reference frame:

Table 5. 1

$x_i = [15\ 15]$
$x_d = [65\ 15]$
$x_{O1} = [28\ 14]$
$x_{O2} = [44\ 13]$
$R_{o1} = R_{o2} = 1.5\ [m]$

where x_{O1} and x_{O2} are the obstacle positions, x_i and x_d are initial point and target point respectively expressed in the two-dimensional cartesian space and R_{o1} and R_{o2} are actual radius of the obstacles.

The first step is to define the global minimum of the potential described as the target point and the generation of its potential function expressed as (3.1). In this phase the important parameter to define is σ that determine its intensity.

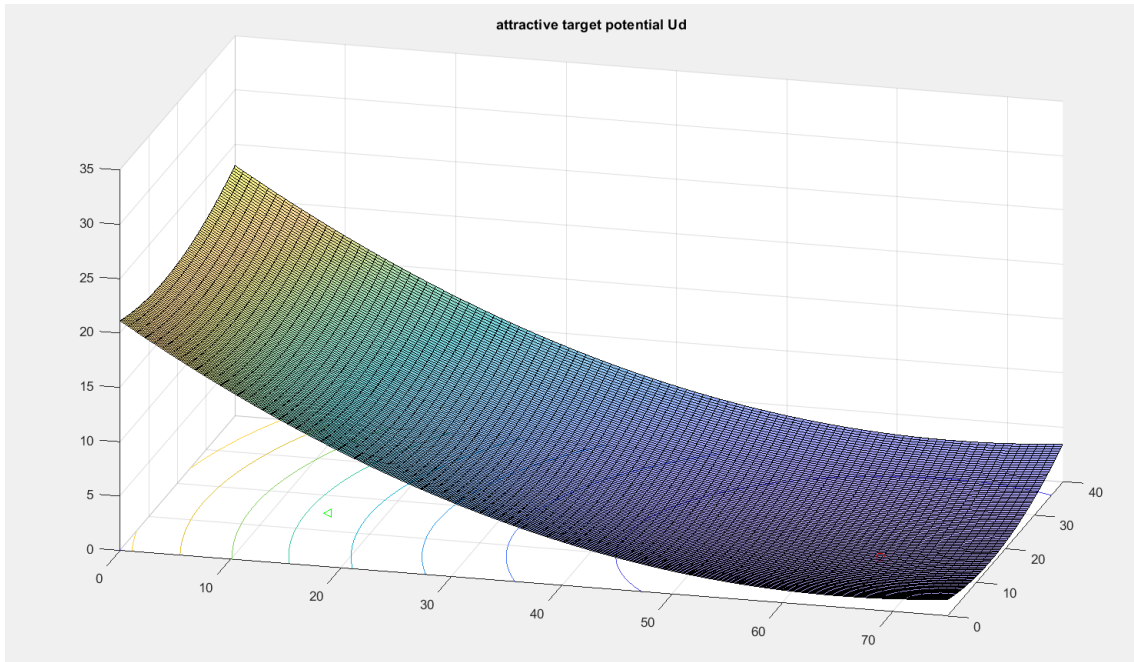Selecting $\sigma = 0.0095$ the result is shown in Figure 5.1

Figure 5. 1: Global minimum potential field.

Before using (3.5) to compute R_o^* it is necessary to compute γ_o as follows:

$$\gamma_o = -\frac{1}{R_o^2} W_{-1} \left(\frac{-v_o^2}{e} \right) \tag{5.1}$$

Then, Table 5.2 shows all the parameters to define the obstacle potential described by (3.2) and are valid for both the obstacles considered in this simulation case.

Table 5. 2

$\beta_o = 5$
$R_o = 1.5 \, [m]$
$\nu_o = 0.3$
$s_\epsilon = 0.01$
$\gamma_o = 2.23$
$R_o^* = 2.68 \, [\text{m}]$

The resultant potential field derived from Table 5.2 values is shown in Figure 5.2a and Figure 5.2b where the resultant shape is the same but differs only from their positions.
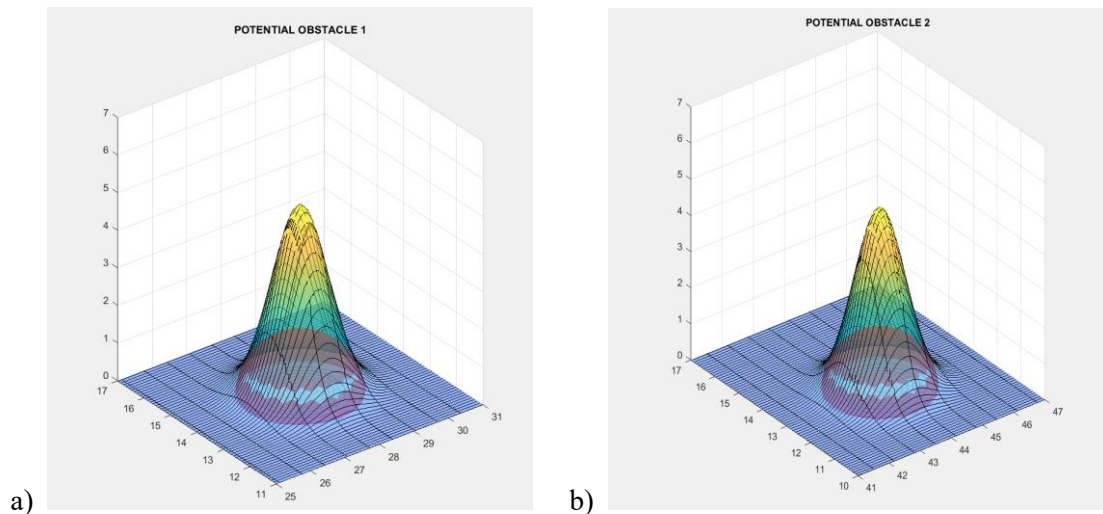

Figure 5. 2 (a-b): Obstacles potential fields.

Furthermore, the local attractor potential field U_a follows the negative exponential function expressed in (3.6). In this scenario its role is crucial since it allows the vessel to be forced to pass by a preferred side of the obstacle considered. As it is shown in Figure 2.1c and Figure 2.1d where are illustrated the overtaking and head-on situations, it is stated from rules 13 and 14 of the COLREGs that: 'When two power-driven vessels are meeting on reciprocal or nearly reciprocal courses so as to involve risk of collision each

shall alter her course to starboard so that each shall pass on the port side of the other'. Consequently, the local attractor it has been positioned on the left side of each obstacle at certain distance to fulfil conditions (3.9) and (3.15) discussed in Chapter 3.

5.1.1 Local Attractor 1

The attractor in a first stage it is being placed at a distance equal to the double of the diameter of the obstacle with an inclination towards the left side of 61° with respect to the vertical axis. Then it is computed the distance:

$$x_a' = ||x_a - x_d|| \tag{5.2}$$

and it is selected a value of γ_a that verify the following condition:

$$x_a' = \sqrt{\frac{27}{4\gamma_a}} \tag{5.3}$$

Further, following equations (5.4) and (5.5) it is possible to compute all the necessary variables to obtain the optimal value of α_a for which no local stationary point occurs during the gradient tracking method application.

$$\theta(x_a', \gamma_a) = \cos^{-1}\left(\frac{27}{2\gamma_a x_a'^2} - 1\right) \tag{5.4}$$

$$\tilde{x}'(x'_a \gamma_a) = \frac{2}{3}x_a'\left[\cos\left(\frac{\theta + 4\pi}{3}\right) + 1\right] \tag{5.5}$$

Substituting (5.4) and (5.5) in (3.12) it results:

$$\tilde{\alpha}_a(\sigma, x_a', \gamma_a) = \frac{-\sigma\tilde{x}'}{\gamma_a(\tilde{x}' - x_a')e^{\frac{-\gamma_a}{2}(\tilde{x}' - x_a')^2}} \tag{5.6}$$

Now, following (3.14) the shifting ε can be calculated to verify condition (3.9) and following (3.7) can be find R_a^* and verify (3.15). It is verified that:

$$||x_a - x_{o1}|| = 6.075 \ [m] > R_o^* + \varepsilon = 2.6779 + 3.3967 = 6.074 \ [m]$$

This procedure it is necessary for the first attractor since the second condition shown in Figure 3.5 it is true as it is illustrated in Figure 5.6.

5.1.2 Local Attractor 2

The second local attractor it is being placed at a distance equal to 3 times the radius of the obstacle with an inclination towards the left side of 40° with respect to the vertical axis. This leads to verify the first condition of Figure 3.5 as it is shown in Figure 5.6 where the red line which connect the x_{a1} and x_{a1} points to the target point demonstrate that the intersection of the segment relative to the second attractor with the circle described by R_{o2}^* is empty. So, in this case it is not necessary to verify condition (3.9) and the R_a^* referred to the second attractor can be freely selected. Aside from this, the procedure to be followed for the second attractor does not differ from the previous paragraph. So, in the following Tables are listed all the parameters relative to the two different potential fields able to generate the negative exponential function showed in Figure 5.3 and in Figure 5.4 together with the correspondent obstacle potentials.

Table 5. 3

$\gamma_a = 0.463$
$x_a' = 42.5\ [m]$
$R_a^* = 7.59\ [m]$
$\alpha_a = 1.71$
$\varepsilon = 3.397$

Table 5. 4

$\gamma_{a2} = 0.463$
$x_{a2}' = 24.5\ [m]$
$R_{a2}^* = 5.25\ [m]$
$\alpha_{a2} = 0.42$

Then in Figure 5.5 is represented the total potential field U_t to be used in the control law expressed in equation (4.9), which in this case can be formulated as:

$$U_t(x) = U_d(x) + U_{o1}(x) + U_{a1}(x) + U_{o2}(x) + U_{a2}(x) = \quad (5.7)$$

$$= \frac{1}{2}\sigma||x - x_d||^2 + \beta_{o1}e^{-\frac{\gamma_{o1}}{2}||x-x_{o1}||^2} - \alpha_{a1}e^{-\frac{\gamma_{a1}}{2}||x-x_{a1}||^2} + \beta_{o2}e^{-\frac{\gamma_{o2}}{2}||x-x_{o2}||^2}$$

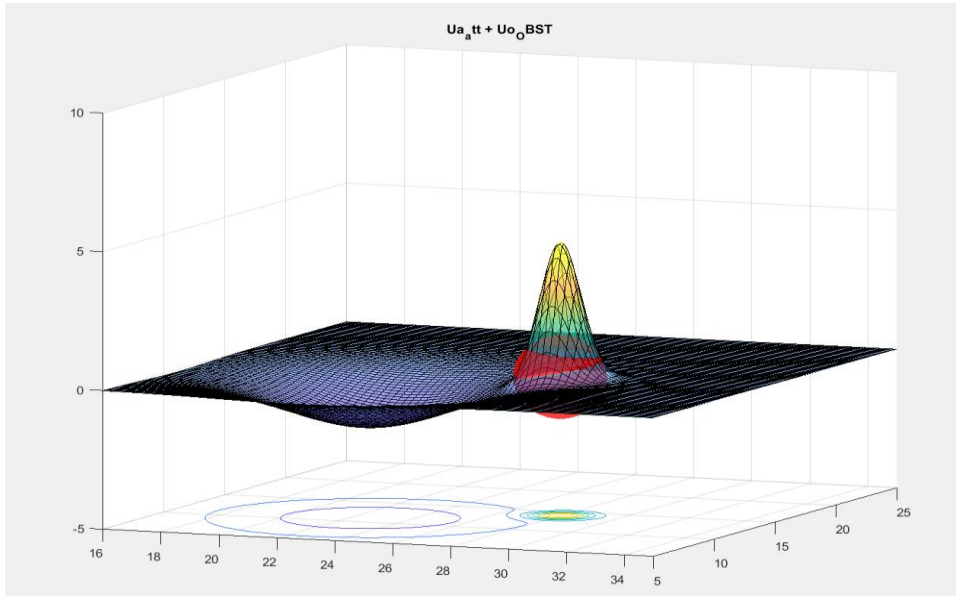$$- \alpha_{a2}e^{-\frac{\gamma_{a2}}{2}||x-x_{a2}||^2}$$

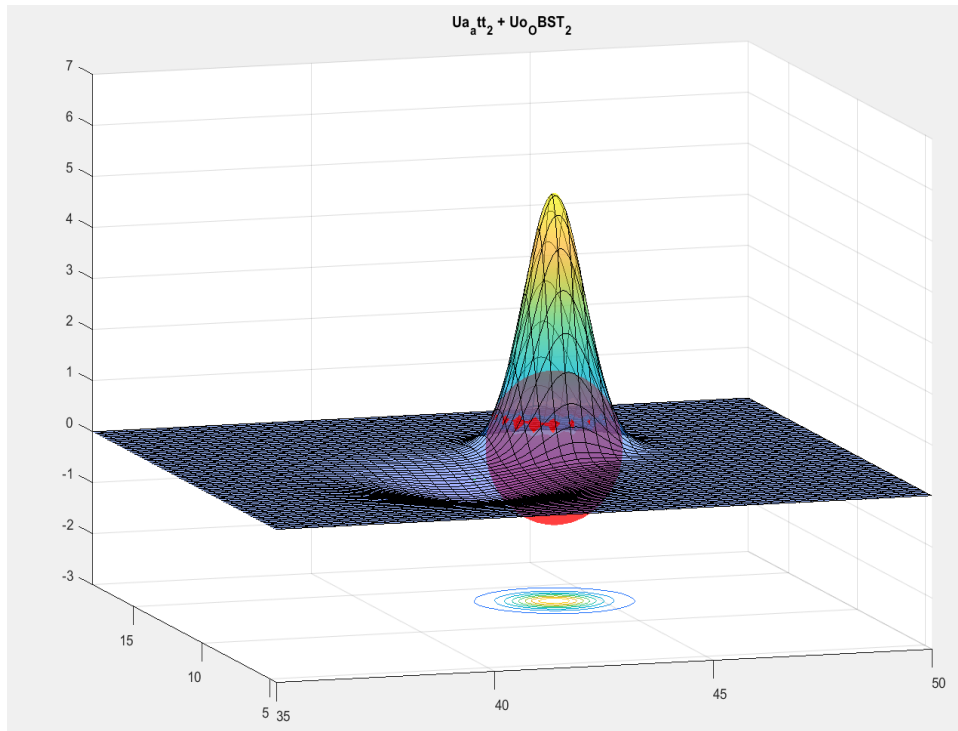**Figure 5. 3:** Obstacle n°1 and local attractor n°1 potential field.

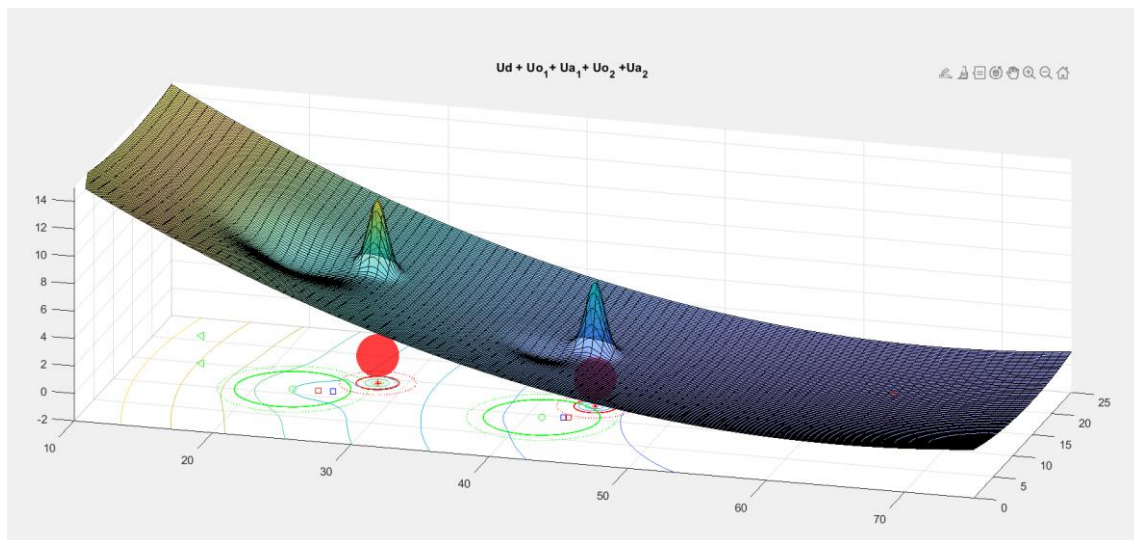**Figure 5. 4:** Obstacle n°2 and local attractor n°2 potential field.

Figure 5. 5: Graphical representation of total potential field U_t.

Subsequently, to proceed with the control strategy it is necessary to consider the gradient lines generated from this scenario since the force to be applied to the USV are strictly dependent from them as it is shown in Figure 5.6. In this test, that now on will be referred as Test 1, it is stressed the influence of the local attractor positioning the first

obstacle with a vertical coordinate $y_{o1} = 14$ [m] to suggest a predictable and advantageous choice of the side of approach opposite to the one with the attractor.
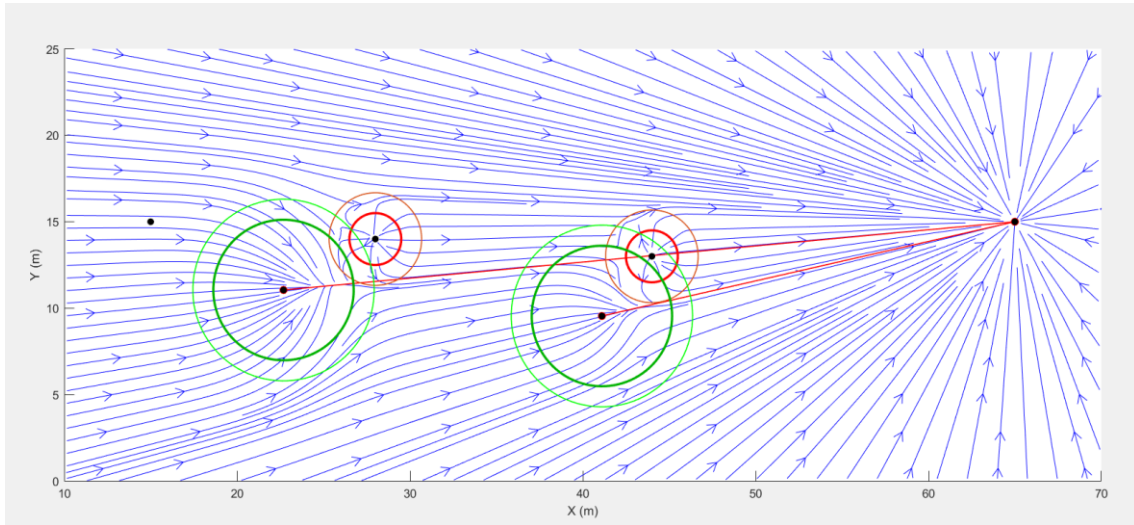

Figure 5. 6: Graphical representation of obstacles and local attractors with gradient lines.

Moreover, Test 1 it has been conducted with a sampling time referred to the integration of the differential equations that describe the dynamic of the boat of Ts = 6.1 [s] and a proportional constant value of K = 6.9 (3.12). It has been experimented that high value of this constant makes the control more effective since it increases the steering action, but an excessive value makes the system unstable and produce an unpredictable behaviour. These values are obtained from trial-and-error procedure conducted in Matlab software during simulations.

Finally, in terms of path generation Figure 5.7 shows how the USV trajectory generated by the APF control strategy compared with the trajectory generated by the NMPC controller settled as it is described in this thesis work [20] with obstacle dimensions and positions described before for both cases. The inner ellipse, in black, is the actual size of the obstacle and the outer ellipse, in green, is the inflated ellipse considering the boat's dimensions so that the collision is avoided if the trajectory line does not enter the green circle. Moreover, considering the overtaking situation only the first method can ensure COLREGs compliance.
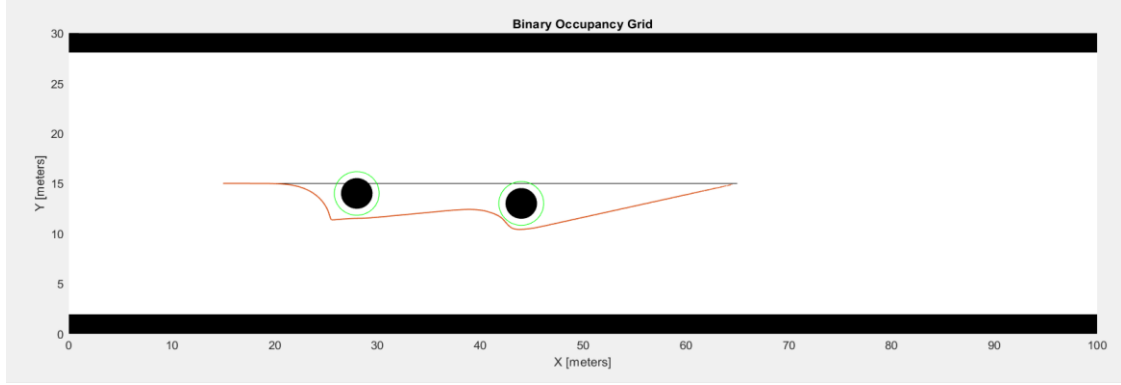
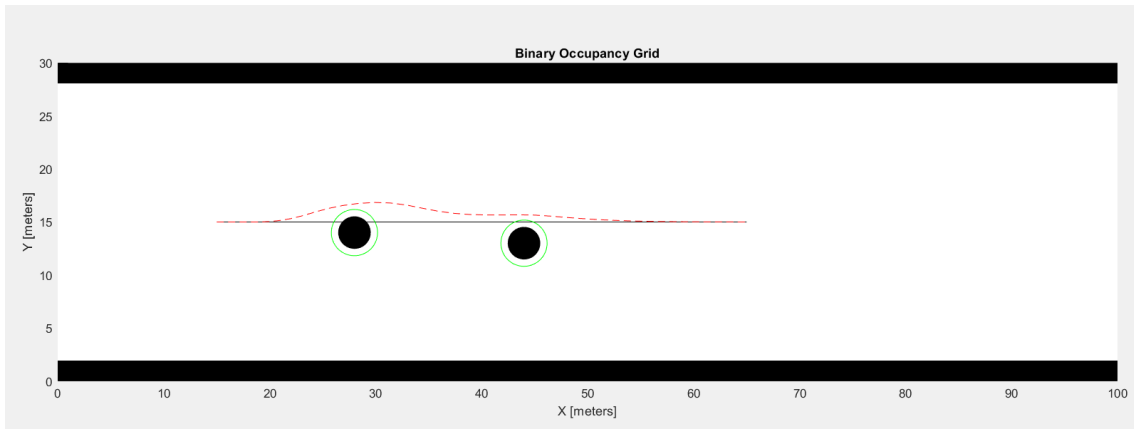**Figure 5. 7:** Artificial potential filed controller path generation.

Figure 5. 8: NMPC controller path generation.

5.2 Dynamic Obstacle

Test 2 has been conducted aiming in reproducing a head-on situation where an USV is frontally approaching the other at a certain speed. In this case it is considered for simplicity the same size of the obstacle previously examined in Test 1 and a cruise velocity of 1.2 m/s since this is near the limit on Venice's canals. Instead, the global attractor is modelled considering $x_d = [50\ 6.5]^T$ and $\sigma = 0.03$. Regarding the obstacle and local attractor potential field, parameters used to model their functions have not changed. Although, the local attractor is positioned at a distance equal to 3.4 times the radius of the obstacle and oriented toward the left with respect to the vertical axis of 50°.

 Moreover, since the strictly dependence of $\tilde{\alpha}_a$ from the actual position of the obstacle (5.6) and subsequently of the local attractor, it must be computed iteratively for each

control step. This procedure ensure that no local minima is created during the path progression. Simulation is conducted with a control frequency of 30 Hz since it is close to the frequency used by the sensors on board of the USV, while the sampling time interval chosen for the dynamic model solver is $Ts = 6[s]$.

Table 5. 5

$\gamma_a = 0.27$
$x_a' = 48.6\,[m]$
$R_a^* = 7\,[m]$

Furthermore, in the control strategy it has been found an optimal proportional control value of $K = 8.1$.
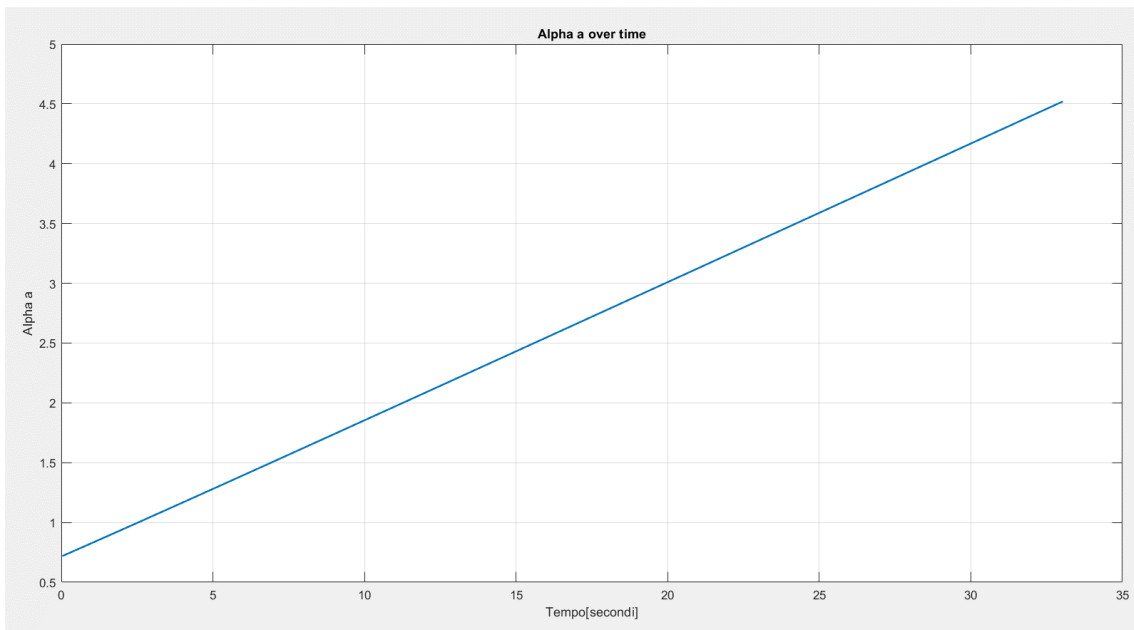

Figure 5. 9: $\widetilde{\alpha}_a$ variation over simulation time.

In conclusion, the resultant collision avoidance trajectory generated from the control strategy proposed is compared, as before, with the NMPC methodology in figure 5.10. It highlights the compliance of rule 14 of COLREGs in the case of APF application despite of a less smooth behaviour with respect to the other generated path whose side of approach cannot be directly controlled.

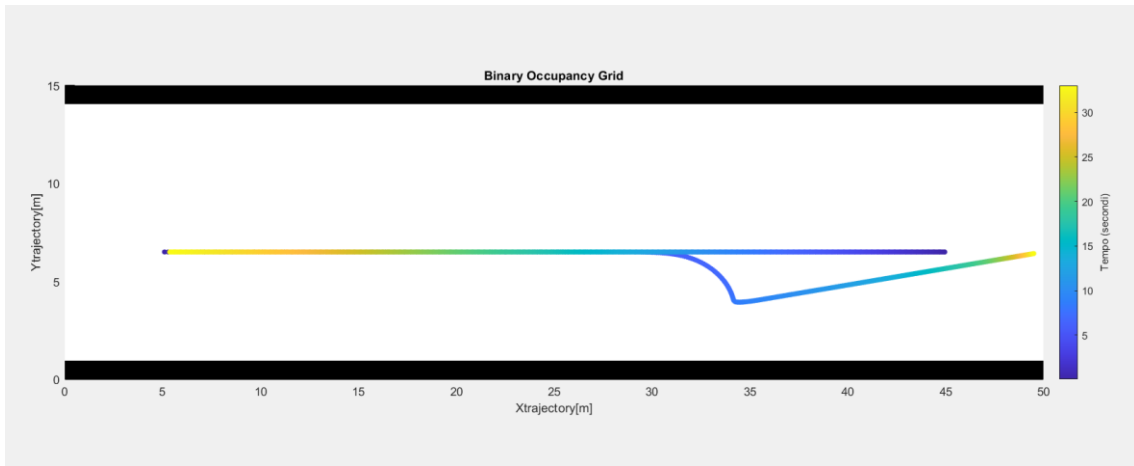**Figure 5. 10:** APF trajectory generated of the USV compared to the obstacle trajectory.
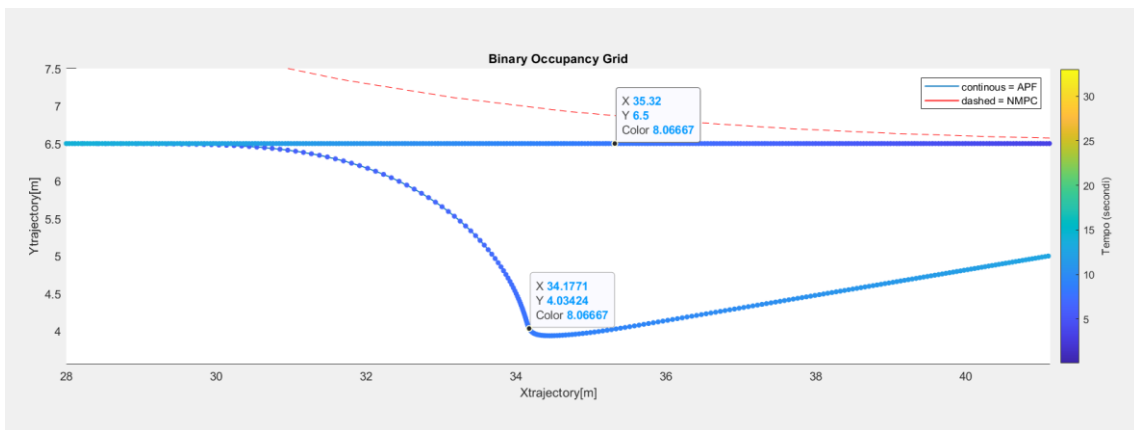
Figure 5. 11: Closer view of the dynamic obstacle where color stands for the time instant of the relative position assumed from the USV and the obstacle, that clearly demonstrates that the collision avoidance is fulfilled since at the same time instant their positions are sufficiently far away from each other.

Figure 5. 12: Comparison of APF (continuous line) trajectory and NMPC (dashed line) trajectory with the same approaching obstacle represented by the continuous line that start from [45, 6.5] and ends in [5, 6.5].

Chapter 6

Conclusions
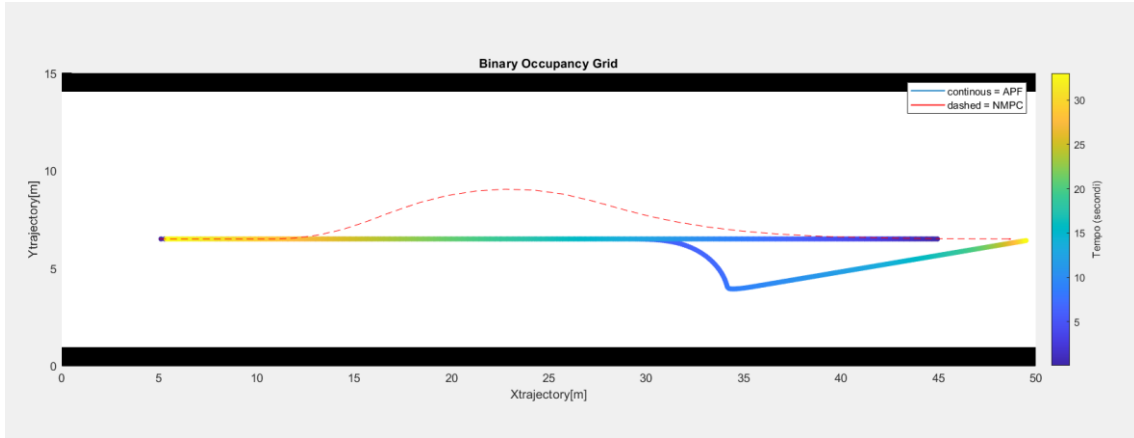
The objective of this thesis was to apply a methodology able to replace human intervention in maritime navigation in presence of static and dynamic obstacles operating on urban canals with COLREGs compliance. This task raised the question of which is the most suitable control strategy able to fulfil the requirements specified. The work started considering a NMPC control strategy with good performance in sense of path planning and trajectory tracking. One issue of the controller design is that it is not COLREGs compliant, with violations present in Figure 5.8 and Figure 5.12. For this reason, the design of an Artificial Potential Field strategy with the use of local attractors it has been developed. The first step was to suitably tune the parameters of both the repulsive and the attractive potentials to obtain a total potential field where no local minima occur. Therefore, the control strategy chosen exploits the negative gradient of the potential as control input in terms of force to be applied to the boat's thrusters. To do so, the error angle between the direction of the gradient computed in the following control step and the actual yaw angle of the boat is chosen as variable to evaluate the best control input to steer the boat. This variable is tuned by means of a proportional gain. While the magnitude of the gradient is chosen as the control input responsible for guiding the boat in forward direction. In both cases of static and dynamic obstacles the controller was able to accomplish the given tasks:

- Follow a collision free path generated through the gradient lines extrapolated from the potential field.
- Follow the preferred direction highlighted by the local attractor to be COLREGs compliant in the two different case scenarios.
- Drive the boat from a defined starting point to a goal configuration with near zero error.

In addition, the obtained performance can be considered acceptable in terms of task requirements but at the cost of a bigger boat's jerk that reduces comfort for passengers with respect to the NMPC strategy that keeps the trajectory smoother. This is caused by

the necessity of being sufficiently close to the obstacle to being able to sense the attractive source to adjust the trajectory and steer the boat.

6.1 Future Work

To improve the work done in this thesis, the following proposition could be implemented:

- The current implementation was done on MATLAB, but it would be ideal to implement it in a compiled programming language such as C++ exploiting it in a simulation environment such as ROS or similar.
- In this work only two of the four COLREGs manoeuvres showed in Figure 2.1 have been tested, so it could be useful to evaluate the performance of this strategy also in the case of the crossing from right and crossing from left situation to have a better understanding of the relevance of this application.

Bibliography

[1]   Anete Vagale, Rachid Oucheikh, Robin T. Bye, Ottar L. Osen, and Thor I. Fossen. «Path planning and collision avoidance for autonomous surface vehicles I: a review». In: Journal of Marine Science and Technology (Japan) 26 (4 Dec. 2021). Definition of COLReg, path planning and trajectory planning. List of many path planning algorithms incuding sampling based, pp. 1292–1306. issn: 09484280. doi: 10.1007/ s00773-020-00787-6 (cit. on pp. 3, 5, 14).

[2]   Miao, T., El Amam, E., Slaets, P., & Pissoort, D. (2022). An improved real-time collision-avoidance algorithm based on Hybrid A* in a multi-object-encountering scenario for autonomous surface vessels. *Ocean Engineering*, *255*, 111406

[3]   Steven M. LaValle. «Rapidly-exploring random trees: a new tool for path planning». In: The annual research report (1998) (cit. on pp. 3, 8)

[4]   Sertac Karaman and Emilio Frazzoli. «Sampling-based Algorithms for Optimal Motion Planning». In: (May 2011). Pseudocodes for RRT and RRT* algorithms. Paper where RRT* is introduced as well as its characteristics about convergence and optimality. url: http://arxiv.org/abs/1105.1186 (cit. on pp. 4, 9).

[5]   Sertac Karaman, Matthew R. Walter, Alejandro Perez, Emilio Frazzoli, and Seth Teller. «Anytime motion planning using the RRT». In: 2011, pp. 1478–1483. isbn: 9781612843865. doi: 10.1109/ICRA.2011.5980479 (cit. on pp. 4, 10, 11).

[6]   Chen, L., Mantegh, I., He, T., & Xie, W. (2020, September). Fuzzy kinodynamic RRT: a dynamic path planning and obstacle avoidance method. In 2020 international conference on unmanned aircraft systems (ICUAS) (pp. 188-195).

[7]   Chinmay Vilas Samak, Tanmay Vilas Samak, and Sivanathan Kandhasamy. «Control Strategies for Autonomous Vehicles». In: (Nov. 2020). url: http://arxiv.org/ abs/2011.08729 (cit. on p. 4).

[8]   O. Khatib. «Real-time obstacle avoidance for manipulators and mobile robots». In: Institute of Electrical and Electronics Engineers Inc., 1985, pp. 500–505. isbn: 0818606150. doi: 10.1109/ROBOT.1985.1087247 (cit. on p. 4).

[9]   J. van den Berg, M. Lin, and D. Manocha, "Reciprocal velocity obstacles for real-time multi-agent navigation," in Proc. IEEE Int. Conf. Robot. Autom., 2008, pp. 1928–1935.

[10]   C. Fulgenzi, A. Spalanzani, and C. Laugier, "Dynamic obstacle avoidance in uncertain environment combining PVOs and occupancy grid," in Proc. IEEE Int. Conf. Robot. Autom., 2007, pp. 1610–1616

[11]   Kuwata, Y., Wolf, M. T., Zarzhitsky, D., & Huntsberger, T. L. (2013). Safe maritime autonomous navigation with COLREGS, using velocity obstacles. IEEE Journal of Oceanic Engineering, 39(1), 110-119.

[12]   Hagen, I. B., Kufoalor, D. K. M., Brekke, E. F., & Johansen, T. A. (2018, May). MPC-based collision avoidance strategy for existing marine vessel guidance systems. In 2018 IEEE International Conference on Robotics and Automation (ICRA) (pp. 7618-7623).

[13]   Trym, T., Brekke, E. F., & Johansen, T. A. (2020). On collision risk assessment for autonomous ships using scenario-based MPC. IFAC-PapersOnLine, 53(2), 14509-14516.

[14]   Beard, R., & McClain, T. (2003). Motion planning using potential fields. Brigham Young University, BYU ScholarsArchive, Faculty Publications 1313. Retrieved from http://www.et.byu.edu/~beard/papers/preprints/ BeardMcLain03-potential.pdf

[15]   J. Latombe, Robot Motion Planning. Norwell, MA: Kluwer Academic, 1991, pp. 295–310

[16]   Melchiorre, M., Scimmi, L. S., Salamina, L., Mauro, S., & Pastorelli, S. (2022). Robot collision avoidance based on artificial potential field with local attractors. In Proceedings of the ICINCO.

[17]   Perez, T. (2006). Ship motion control: course keeping and roll stabilisation using rudder and fins. Springer Science & Business Media.

[18]   Wei Wang, Tixiao Shan, Pietro Leoni, David Fernandez-Gutierrez, Drew Meyers, Carlo Ratti, and Daniela Rus. «Roboat II: A Novel Autonomous Surface Vessel for Urban Environments». In: (July 2020). url: http://arxiv.org/abs/2007.10220 (cit. on p. 33).

[19]   Güldner, J.; Utkin, V.I. Tracking the gradient of artificial potential fields: Sliding mode control for mobile robots. Int. J. Control 1996, 63, 417–432.

[20]   Vinicius Massaki Benevides Kanaoka, Trajectory Planning and Motion Control of Autonomous Electric Boats. Politecnico di Torino, Corso di laurea magistrale in Ingegneria Informatica (Computer Engineering), 2023.

[21]   Shaorong Xie et al, "The obstacle avoidance planning of USV based on improved artificial potential field," in IEEE International Conference on Information and Automation (ICIA), Hailar, China, 2014, pp. 746–751.